

# The effects of thin film homogeneity on the performance of ferroelectric tunnel junctions

A Dörfler<sup>1,2</sup> , G Kolhatkar<sup>2</sup> , U Wagner<sup>2</sup> and A Ruediger<sup>1</sup>

<sup>1</sup> INRS-EMT, 1650 Blvd. Lionel-Boulet, Varennes (Québec), J3X 1S2, Canada

<sup>2</sup> Department of Applied Sciences and Mechatronics, Munich University of Applied Sciences, 80335 Munich, Germany

E-mail: [andreas.doerfler@emt.inrs.ca](mailto:andreas.doerfler@emt.inrs.ca)

Received 7 November 2019, revised 17 December 2019

Accepted for publication 17 January 2020

Published 6 February 2020



## Abstract

The compelling physical properties of the recently discovered ferroelectric phase in thin film  $\text{Hf}_x\text{Zr}_{1-x}\text{O}_2$  have opened a window for applications such as non-volatile resistive switching memory devices with high retention known as ferroelectric tunnel junctions. In this article, we investigate the stability of these two-terminal, polarization induced resistance-switching devices with respect to the statistical reproducibility of constitutive electrical parameters based on surface thickness inhomogeneities. We provide a straightforward, quantitative model to estimate tunneling currents dependent on thickness variations, and the resulting tunneling electroresistance (TER) ratios and breakdown probability. An analytical expression for the probability distribution of tunneling currents for normally distributed thicknesses is given. Using material parameters of a TiN/HZO/Pt heterostructure, practical design requirements are deduced and an estimation with respect to the surface roughness is given for practical ferroelectric layer thicknesses and voltages below 4 nm and 1 V, respectively. In this regime, the simple model of a ballistic, direct tunneling mechanism can be used to adequately model the thickness and voltage dependence of the resistivity.

Keywords: ferroelectricity, tunnel junction, HZO, thin film,  $\text{HfO}_2$

(Some figures may appear in colour only in the online journal)

## 1. Introduction

The discovery of a ferroelectric phase in  $\text{Hf}_x\text{Zr}_{1-x}\text{O}_2$  (HZO) thin films published by Bösccke *et al* [1] has opened a unique prospect for integration in commercial memory devices. The material's ferroelectric properties, compatibility with silicon and CMOS technology as well as its high dielectric constant has made thin film HZO a promising candidate in the field of ferroelectric random-access memory (FeRAM), Resistive RAM (ReRAM) [2, 3] and artificial neural networks [4–7]. Polarization retention, switching durability, as well as the predictability and reproducibility of electrical characteristics are especially crucial for integrated systems. Consequently, a large amount of research is being conducted to understand and bring ferroelectric devices to a competitive level with existing technology.

While traditional ferroelectric bulk materials like barium titanate ( $\text{BaTiO}_3$ ) or lead zirconate titanate (PZT) [8] lose their ferroelectricity in thin film form, HZO requires a nanometer scale film thickness to form its ferroelectric phase [9, 10]. This enables the creation of ferroelectric tunnel junctions (FTJs). FTJs have been identified as one of the most promising candidates to challenge DRAM. They have a simple structure, consisting of two electrodes separated by a nanoscale ferroelectric layer. This layer represents a potential barrier that restricts the transport of charge carriers to tunneling. Using two different electrode materials, a polarization dependent asymmetry in the barrier potential is generated. This causes a modulation of the tunneling probability upon polarization reversal, creating a low resistance state (LRS) and a high resistance state (HRS) for the two polarization directions. This phenomenon is known as Tunneling Electroresistance (TER). The first fully

CMOS-integrable FTJ, built from a TiN/HZO/Pt heterostructure, was reported by Ambriz-Vargas *et al* [11]. These device uses ferroelectric HZO as the potential barrier and TiN as a bottom electrode. The latter is also an oxygen diffusion barrier between silicon and HZO, that requires moderate deposition temperature and provides good electrical conductivity [12].

For HZO insulator thicknesses below 4 nm, operating voltages below 1 V and moderate temperatures, the dominant conduction mechanism can be described by the direct tunneling (DT) model [8, 13]. Higher voltages require the Fowler–Nordheim Tunneling description, while at higher thicknesses, the temperature driven thermionic emission prevails [14, 15]. Readout is accomplished by probing the resistivity state at sub-coercive voltages. The tunneling current can be described by the Wentzel–Kramers–Brillouin (WKB) approximation, which describes the tunneling probability through a trapezoidal potential barrier, neglecting screening effects in the electrodes. The WKB formula provides a thickness and voltage dependent analytical approximation of the tunneling currents. According to this approximation, the tunneling current exponentially rises with decreasing thickness. To switch the polarization, a coercive electric field making up a significant fraction of the breakdown voltage is required. This implies the risk of inducing defects that deteriorate device performance. Thus, thickness variations in the thin film on an atomistic scale pose a significant risk of locally exceeding the breakdown field.

Deposition dependent as well as growth mode induced topological fluctuations on the bottom electrode and the ferroelectric, as well as the polycrystalline nature of HZO necessarily yield a statistical distribution of oxide thickness and the corresponding potential barrier width, leading to large variations in the tunneling currents over the surface. Due to the exponential dependence of tunneling with respect to the barrier thickness, a thickness reduction by a single unit cell (from 3 nm to 2.5 nm) induces an increase in the conductivity by 3 orders of magnitude for the investigated device. Therefore, a quantitative statistical description of electrical parameters dependence on thickness fluctuations is critical to the device performance. In this work, we provide a simple model that allows us to quantify the effects of thickness changes in a TiN/HZO/Pt heterostructure such as the one described in [11]. We focus on the TER induced by the modulation of the respective barrier heights. For metallic electrodes, screening effects that modulate the barrier width are considered small due to the high electron density in the conduction band.

## 2. Methods

The derivations employ the WKB approximation as a basis to quantify the effects of inhomogeneities in the ferroelectric layer. We describe a three-layer TiN/HZO/Pt structure with a 3 nm ferroelectric layer that is operated within the limits of the trapezoidal WKB model, which we separate into analytical small and large voltage approximations. These equations allow the derivation of a closed form expression for the distribution of current densities, given an arbitrary distribution of tunneling barrier thicknesses.

Numerical consistency checks, evaluations and plots were performed using the numerical computing language Julia [16]. The analytic formulations were checked using the symbolic algebra library SymPy [17].

The ferroelectric phase in HZO deposited by atomic layer deposition or sputtering processes has been attributed to the film's polycrystalline grain structure [10]. While HZO films much thicker than 10 nm are mostly composed of the non-ferroelectric cubic and tetragonal structures, smaller thicknesses increasingly favor the formation of the ferroelectric orthorhombic phase.

A polycrystalline film with a thickness in a range of 2 nm to 4 nm inherently induces significant relative thickness fluctuations in the ferroelectric layer. Imperfections in the surface homogeneity of the base electrode may exacerbate this effect. Magnetron-sputtered TiN/HZO/Pt heterostructure with an HZO thickness of 2.8 nm exhibit an rms surface roughness of 0.2 nm on the TiN bottom electrode, and 0.1 nm on the thereon deposited HZO [11]. This results in thickness variations in the HZO film. To understand the impact of this inhomogeneity, we developed a model that describes the tunneling current behavior in HZO based FTJs using the WKB approximation.

The WKB approximation across a trapezoidal barrier quantifies the current density  $J$  as a function of barrier thickness  $d$  and voltage  $U$ . The analytical expression [8, 18, 19] can be written as

$$J(d) = \frac{C}{d^2} e^{Dd} \times \sinh(Ed), \quad (1)$$

with the parameters  $C$ ,  $D$ ,  $E$

$$C = \frac{4em_e}{9\pi^2\hbar^3} \frac{1}{\alpha^2[p_2 - p_1]^2} \quad (1a)$$

$$D = \alpha [p_2^3 - p_1^3] \quad (1b)$$

$$E = \frac{3}{4} e |U\alpha [p_2 - p_1]| \quad (1c)$$

where  $\alpha$ ,  $p_1$ ,  $p_2$  are given by

$$\alpha = \frac{-4\sqrt{2m_e}}{3\hbar [p_2^2 - p_1^2]}, \quad (1d)$$

and

$$p_{1/2} = \sqrt{\phi_{1/2} \pm eU/2}. \quad (1e)$$

In this equation,  $\phi_1$  and  $\phi_2$  are the trapezoidal interface potential barriers (see figure 1),  $m_e$  the electron mass, and  $U$  and  $d$  are the operating voltage and thickness, respectively.

Using  $\phi_{1,2}$  as shown in table 1, and equation (1), the  $J$ – $V$  curves in the HRS and LRS were reconstructed for a 3 nm HZO film, as illustrated in figure 3 (gray curves). The  $J$ – $V$  curve follows a large exponential slope that tapers off into a shallower linear exponential. At higher voltages, the current density increases exponentially with the voltage. To represent these two regions, the approximations  $\sinh(Ed) \approx Ed$  and  $\sinh(Ed) \approx \frac{1}{2}e^{Ed}$  were used, which approximate the regions for  $U$  smaller and larger than  $\log(2)/E$ , respectively. The

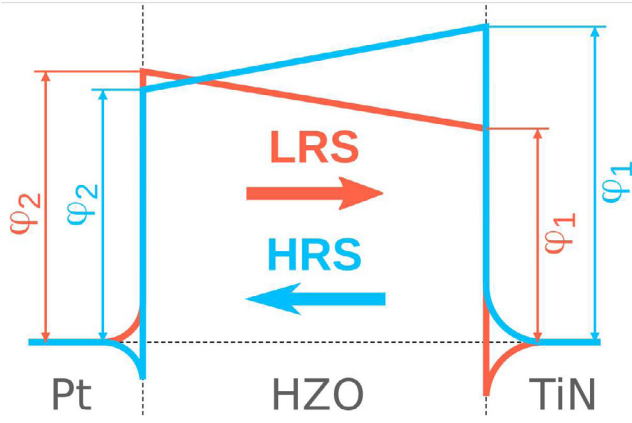


**Figure 1.** Modulation of potential barrier for the low resistance state (LRS), where the polarization is in the direction of the TiN interface (red), and the high resistance state (HRS), where the polarization is oriented towards of the Pt interface (blue).

**Table 1.** Potential barriers  $\phi_{1,2}$  at TiN and Pt interfaces for HRS and LRS polarization states according to Ambriz-Vargas *et al* [11].

Material	TiN	Hf <sub>0.5</sub> Zr <sub>0.5</sub> O <sub>2</sub>	Pt
Property	$\phi_1$ (eV)	Polarization	$\phi_2$ (eV)
HRS	2.75	Towards Pt	2.20
LRS	1.86	Towards TiN	2.36

current density of equation (1) is split into the two following equations:

$$J_s(d) \approx \frac{CE}{d} e^{dU} \text{ for } U < \log(2)/E, \quad (2a)$$

$$J_l(d) \approx \frac{C}{2d^2} e^{(D+E)d} \text{ for } U > \log(2)/E. \quad (2b)$$

### 3. Results

A comparison between the WKB model equation (1) and the approximations (2a) and (2b) is shown in figure 3 (gray line with green and red approximations, respectively). The calculations and figures are shown exemplary for a ferroelectric film thickness of 3 nm. Limiting factors for the thickness are prohibitively high resistivity for larger thicknesses for acceptable readout speed, and electrical instability/breakdown for smaller thicknesses. A good agreement is obtained in each region, showing that for a barrier width of  $d = 3$  nm, the WKB formula is accurately described by the approximations, as long as each approximation is used within its threshold of  $U = \log(2)/E$  (blue vertical lines). These approximations can be exploited to calculate the current density distribution in a closed form in the next section.

Using these approximations, the exponential dependency of the current density on both barrier width and operating currents can be calculated for the LRS and HRS, respectively. For both LRS and HRS, the current density increases exponentially when decreasing the HZO thickness. Also, the current density increases exponentially with the voltage above a certain threshold, consistent with the curves shown in

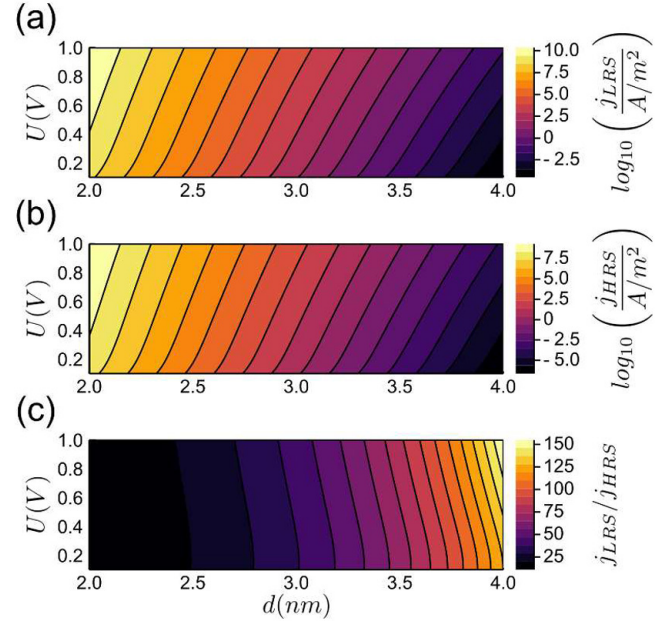


**Figure 2.** Semi-logarithmic plots of the effect of the voltage and the HZO thickness on the (a) LRS current density, (b) HRS current density, and (c) linear plot of the TER ratio of LRS and HRS current densities. Tunneling currents are calculated from equation (1). Over varying thickness and voltages. Increasing voltage and thickness improves the TER.

figure 3. [20] The ratio between the two is critical for distinguishing the two resistive states and is known as the tunneling electroresistance (TER) ratio. It can be defined as the ratio of current densities

$$\text{TER} = \frac{j_{\text{LRS}}}{j_{\text{HRS}}}. \quad (3)$$

The TER ratio grows with voltage and barrier width. A plot of the LRS, HRS and TER over voltage and material thickness is shown in figures 2(a)–(c). Higher currents are beneficial for a fast readout of the resistivity state, which is assisted by lower thicknesses. In addition, the voltage is limited by the breakdown threshold of the device. Therefore, the TER ratio can be optimized by adjusting the HZO thickness while remaining below the device breakdown voltage, neglecting the effect of roughness induced field enhancement [21]. In the equations (1)–(3), variations of the HZO thickness are not yet taken into consideration.

To account for these effects, we model the FTJ device as a series of parallel resistors with resistances dependent on the local film thickness (see figure 4). Since the total resistance is predominantly defined by the smallest parallel resistance, the distribution of thicknesses is crucial parameter.

The effect of varying local film thicknesses, and therefore the film surface roughness, on the current density is thus crucial in understanding the total device conductance. Since the current density  $J$  is a monotone function with respect to  $d$ , its probability distribution  $pdf_J(j)$  for a distribution of thicknesses  $pdf_d(d)$  can be expressed as [22]

$$pdf_J(j) = pdf_d(J^{-1}(j)) \left| \frac{dJ^{-1}(j)}{dj} \right|, \quad (4)$$

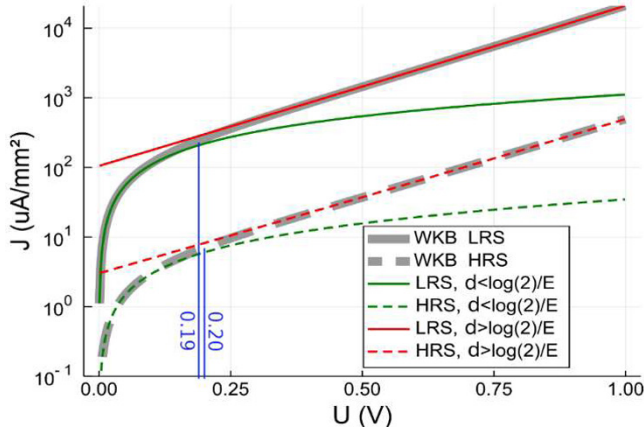


**Figure 3.**  $J$ - $V$  behavior in the HRS (dashed line) and the LRS (full line) according to the WKB approximation (gray), as well as with the small (green) and large voltage approximations (red) for an ideally homogeneous insulator with a thickness of 3 nm. The transition point between the small and large voltage approximation ( $\log(2)/E$ ) is indicated for each curve by the blue line.

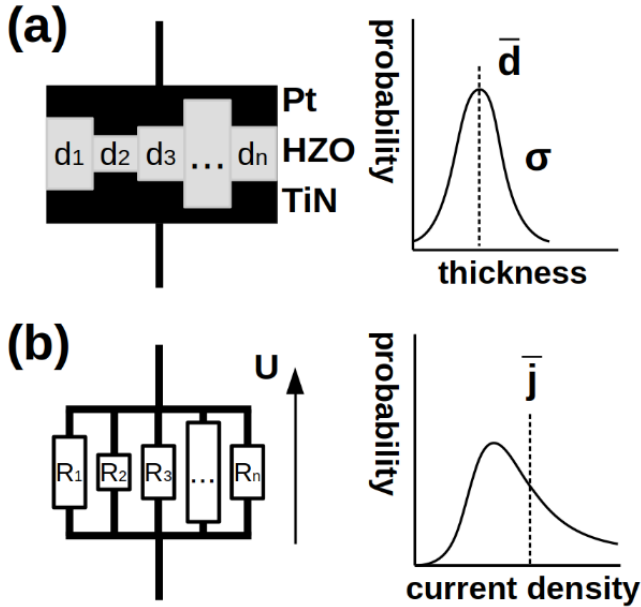


**Figure 4.** HZO conductivity model. The local film thickness results in a local current density at voltage  $U$ . (a) Representation of roughness as a distribution of thicknesses. (b) Parallel resistor model yielding the current density distribution for a fixed voltage.

where  $J^{-1}(j)$  is the inverse of function  $J(d)$ . Using the closed form invertibility of equations (2a) and (2b), this yields the generic distributions

$$pdf_{J_S}(j) = pdf_d\left(\frac{-W_{J_S}}{D}\right) \times \left| \frac{W_{J_S}}{jD(W_{J_S} + 1)} \right| \quad (5a)$$

$$pdf_{J_I}(j) = pdf_d\left(\frac{-2W_{J_I}}{D+E}\right) \times \left| \frac{W_{J_I}}{j(D+E)(W_{J_I} + 1)} \right| \quad (5b)$$

with  $W_{J_S} = W\left(\frac{-CDE}{j}\right)$  and  $W_{J_I} = W\left(\frac{-\sqrt{2}C(D+E)}{4\sqrt{j}}\right)$ , where  $W$  is the principal branch Lambert W function [23]. Assuming a normal thickness probability distribution  $pdf_d$

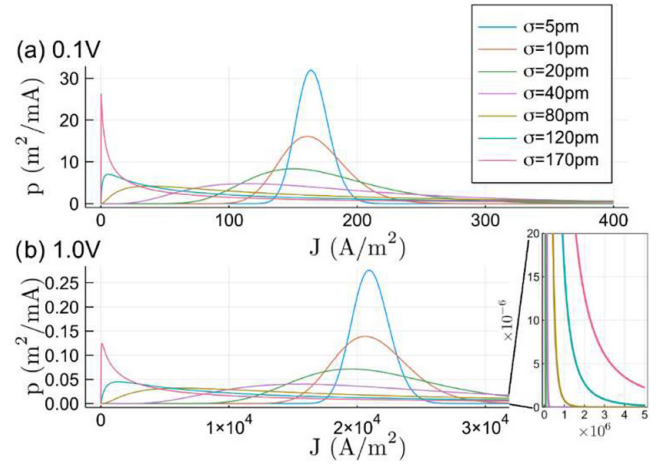


**Figure 5.** Probability density functions of the current density distribution  $pdf_j$  for a mean thickness  $d_0 = 3$  nm and standard deviations between  $\sigma = 5$  pm to 170 pm for (a)  $U = 100$  mV and (b)  $U = 1$  V in the LRS. Although the peak probability moves to lower current densities with increasing  $\sigma$ , the probability distribution increasingly stretches to high current densities as shown in the magnified inset.

$$pdf_d(d) = \frac{1}{\sqrt{2\pi}\sigma^2} \exp\left(-\frac{(d-d_0)^2}{2\sigma^2}\right) \quad (6)$$

for small deviations  $\sigma$  around the mean thickness  $d_0$ , the current density distribution is calculated from equations (5a) and (5b). Both are shown in figures 5(a) and (b) at voltages according to their applicable scope. For  $\sigma = 5$  pm, the current density probability can be described as a narrow Gaussian centered at  $\sim 170 \text{ A m}^{-2}$ . This shows that for such small thickness variations, most of the grain composing the HZO film will depict a tunneling current of  $\sim 170 \text{ A m}^{-2}$ . When  $\sigma$  increases to 10 pm, the current density probability peak decreases by half and becomes broader. As the thickness deviation further increases, the curve becomes broader and the maximum significantly decreases, while shifting to lower current densities. Contrary to the visual shift, the mean conductivity increases in this process, since the distributions increasingly stretch to higher current densities, as shown in the inset on the right-hand side of figure 5(b).

The mean current density through a distribution of parallel grains can be extracted from figure 5 according to the first moments

$$\bar{j} = \int_0^\infty j pdf_j(j) dj. \quad (7)$$

The results of  $j_{LRS}$  and  $j_{HRS}$  for both LRS and HRS are illustrated in figure 6(a) over the thickness standard deviation  $\sigma$ . It shows that the current densities increase exponentially with thickness standard deviation  $\sigma$ . The thickness of the FTJ thus needs to be homogeneous to permit reproducible conductivities. This requirement occurs as the grains function as a parallel resistor network. As a result, the resistance of the network is defined by that of the smallest parallel resistors.

Due to a non-epitaxial film growth of HZO on the bottom electrode, and a crystal structure with a typical lateral grain



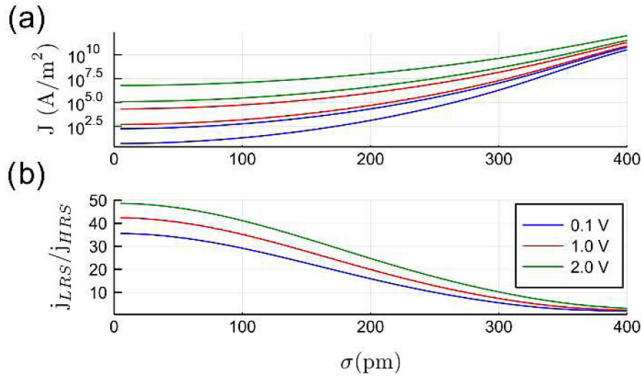


**Figure 6.** (a) Mean current density of LRS state and HRS state for three voltages at a thickness of  $d_0 = 3$  nm. (b) Mean TER ratio over standard deviation. The ratio is stable for small deviations and drops quickly above when  $\sigma$  exceeds  $\approx 0.1$  nm. The TER ratio follows a Gaussian-shaped decay of resistive switching with increasing thickness variations. It can be seen that the thickness inhomogeneity has a significant impact on the TER ratio. This decay results from the fact that the smallest resistances determine the TER, which in return exhibits the lowest TER ratio (figure 2(c)).

size with a size comparable to the film thickness [20, 24, 25], ferroelectric HZO intrinsically exhibits structural thickness variations between the electrode interfaces. As shown in the previous section, this can greatly affect the electrical performance of the device. Another aspect of this analysis is the increased probability of electrical breakdowns. Literature specifications of breakdown voltages in hafnium and zirconium oxide thin films vary between  $7 \text{ MV cm}^{-1}$  and  $20 \text{ MV cm}^{-1}$  [26–29], whereby typical coercive fields require at least  $1 \text{ MV cm}^{-1}$  to  $2.5 \text{ MV cm}^{-1}$  [30, 31]. At this point, higher fields allow increased switching speeds and help switching pinned domains. Switching a 3 nm device by application of 2 V could however already exceed the electric breakdown threshold. Going by these numbers, just approaching the coercive field could already reach 13% to 36% of the breakdown field. Defects in the HZO narrowing the barrier can thus increase the likelihood of an electrical breakdown as observed in [32].

Besides the decay of the TER ratio, FTJs are typically operated at voltages within a significant percentage of their electrical breakdown threshold. For an individual site of random thickness, the cumulative probability of failure over the thickness is

$$p_{\text{site}} = \int_0^{\frac{U}{E_{\text{crit}}}} pdf_d(d) dd = \int_0^{\frac{E}{E_{\text{crit}}}} pdf_d(\sigma_n) d\sigma_n \quad (8)$$

where  $E_{\text{crit}}$  is the critical field strength,  $E = U/d_0$  the mean field strength, and  $\sigma_n = \sigma/d_0$  the relative thickness standard deviation. Thus, the accumulated breakdown probability  $p_N$  for a device with  $N$  sites is

$$p_N = 1 - (1 - p_{\text{site}})^N. \quad (9)$$

This relation is detailed in figure 7, showing linear equipotential lines between field  $E$  and standard deviation  $\sigma$ .

We find an increasing chance of breakdown with increasing the operating voltage and decreasing the mean thickness, as

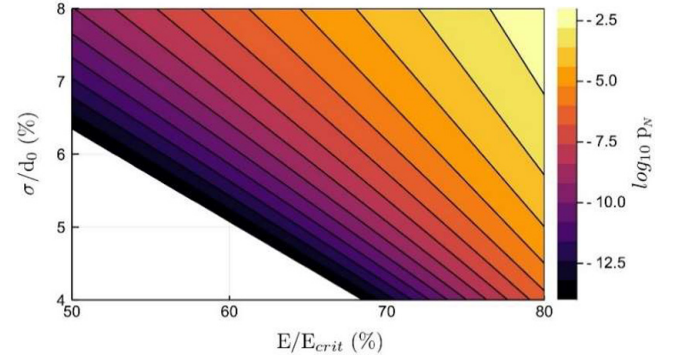


**Figure 7.** Probability of an electrical breakdown in a device  $p_N$ , assuming  $N = 10^6$  statistically independent sites with independent lattice thicknesses. The x-axis measures the mean electric field relative to the critical field  $E/E_{\text{crit}}$  while the y-axis is the relative standard deviation of the thickness  $\sigma/d_0$ . The plot corresponds to a  $3 \mu\text{m} \times 3 \mu\text{m}$  device with an average 3 nm in-plane grain diameter, assuming one statistically independent height per grain.

well as with the device area and the surface roughness. When operating a device with 7% thickness standard deviation at 60% of the critical voltage, 10 out of a million devices will surpass the critical value.

#### 4. Discussion

We investigate the stability of FTJ devices in a TiN/HZO/Pt heterostructure, deriving an analytical formula to allow quantification of the impact of surface roughness on the LRS and HRS resistivity states based on the WKB tunneling model.

Deposition dependent as well as growth mode induced topological fluctuations on the bottom electrode and the ferroelectric, as well as the polycrystalline nature of HZO necessarily yield perturbations in the ferroelectric film thickness. Due to the exponential dependence of tunneling with respect to the barrier thickness, a thickness reduction by a single unit cell (from 3 nm to 2.5 nm) induces an increase in the conductivity by 3 orders of magnitude for the investigated device. Therefore, a quantitative statistical description of the electrical parameters due to thickness fluctuations is critical to understand device performance. Our model allows the quantification of the effects of thickness changes in a TiN/HZO/Pt heterostructure [11], including its effects on the TER ratio. It is important to note that the model is limited to metallic electrodes with negligible screening effects.

#### 5. Conclusion

In summary, we derive a straightforward analytical estimation of the impact of surface roughness on the LRS and HRS state resistivities of ferroelectric tunnel junctions based on the WKB tunneling model. This is exemplified for a TiN/HZO/Pt heterostructure. An exponential increase of conductivity and increased probability of electrical breakdown is quantitatively predicted. We calculate a degradation of the TER ratio with increasing surface inhomogeneities, which is key to reliable information recovery. The high sensitivity of tunneling

currents with respect to the thickness makes this effect critical when investigating device stability. It also means that most of the current will be transferred through a tiny fraction of the ferroelectric domain. Large statistical deviations between individual FTJs must be taken into consideration when planning individual device parameters and global circuitry. Effects due to band structure [33] and field enhancement [21] are neglected at this stage for the sake of clarity but will be included in future studies.

## Acknowledgments

AR gratefully acknowledges funding from an NSERC discovery Grant (RGPIN-2014-05024) and two NSERC strategic partnership grants (506289-2017; 506953-17). GK is thankful for an honorary fellowship of Munich University of Applied Sciences and a postdoctoral fellowship from the Alexander von Humboldt Foundation.

## ORCID iDs

A Dörfler  <https://orcid.org/0000-0003-2177-3697>

G Kolhatkar  <https://orcid.org/0000-0003-0848-4751>

## References

- [1] Böske T S, Müller J, Bräuhäus D, Schröder U and Böttger U 2011 *Appl. Phys. Lett.* **99** 102903
- [2] Yin X, Chen X, Niemier M and Hu X S 2019 *IEEE Trans. Very Large Scale Integr. VLSI Syst.* **27** 159–72
- [3] Boyn S 2016 *PhD Thesis* Université Paris-Saclay, Paris
- [4] Mittermeier B, Dörfler A, Horoschenkoff A, Katoch R, Schindler C, Ruediger A and Kolhatkar G 2019 *Adv. Intell. Syst.* **1** 1900034
- [5] Chen L, Wang T-Y, Dai Y-W, Cha M-Y, Zhu H, Sun Q-Q, Ding S-J, Zhou P, Chua L and Zhang D W 2018 *Nanoscale* **10** 15826–33
- [6] Tian X and Toriumi A 2017 *2017 IEEE Electron Devices Technology and Manufacturing Conf.* (Toyama, Japan: IEEE) pp 36–64
- [7] Stuart T 2019 *Nat. Electron.* **2** 10
- [8] Gruverman A et al 2009 *Nano Lett.* **9** 3539–43
- [9] Polakowski P and Müller J 2015 *Appl. Phys. Lett.* **106** 232905
- [10] Künne C, Materlik R and Kersch A 2017 *J. Appl. Phys.* **121** 205304
- [11] Ambriz-Vargas F, Kolhatkar G, Broyer M, Hadj-Youssef A, Nouar R, Sarkissian A, Thomas R, Gomez-Yáñez C, Gauthier M A and Ruediger A 2017 *ACS Appl. Mater. Interfaces* **9** 13262–8
- [12] Yoon D-S and Roh J S 2002 *IEEE Trans. Electron Devices* **49** 1917–27
- [13] Garcia V and Bibes M 2014 *Nat. Commun.* **5** 4289–301
- [14] Navarro H, Yang I, Sirena M, Kim J and Haberkorn N 2015 *J. Appl. Phys.* **118** 045308
- [15] Pantel D and Alexe M 2010 *Phys. Rev. B* **82**
- [16] Bezanson J, Edelman A, Karpinski S and Shah V 2017 *SIAM Rev.* **59** 65–98
- [17] Meurer A et al 2017 *PeerJ Comput. Sci.* **3** e103
- [18] Soni R, Petraru A, Meuffels P, Vavra O, Ziegler M, Kim S K, Jeong D S, Pertsev N A and Kohlstedt H 2014 *Nat. Commun.* **5** 5414
- [19] Yoon J, Hong S, Song Y W, Ahn J-H and Ahn S-E 2019 *Appl. Phys. Lett.* **6**
- [20] Hyuk Park M, Joon Kim H, Jin Kim Y, Moon T and Seong Hwang C 2014 *Appl. Phys. Lett.* **104** 072901
- [21] Jegert G, Kersch A, Weinreich W and Lugli P 2011 *J. Appl. Phys.* **109** 014504
- [22] Stirzaker D 1999 *Probability and Random Variables: A Beginner's Guide* (Cambridge: Cambridge University Press)
- [23] Dence T P 2013 *Appl. Math.* **04** 887–92
- [24] Wei Y et al 2018 *Nat. Mater.* **17** 1095–100
- [25] Kim H J, Park M H, Kim Y J, Lee Y H, Jeon W, Gwon T, Moon T, Kim K D and Hwang C S 2014 *Appl. Phys. Lett.* **105** 192903
- [26] Chang C-H and Hwu J-G 2009 *IEEE Trans. Device Mater. Reliab.* **9** 215–21
- [27] Mahapatra R, Lee J-H, Maikap S, Kar G S, Dhar A, Hwang N-M, Kim D-Y, Mathur B K and Ray S K 2003 *Appl. Phys. Lett.* **82** 2320–2
- [28] Conley J F, Ono Y, Solanki R, Stecker G and Zhuang W 2003 *Appl. Phys. Lett.* **82** 3508–10
- [29] Li-Mo Wang 2006 *2006 25th Int. Conf. on Microelectronics* (Belgrade, Serbia and Montenegro: IEEE) pp 576–9
- [30] Xu L, Nishimura T, Shibayama S, Yajima T, Migita S and Toriumi A 2017 *J. Appl. Phys.* **122** 124104
- [31] Shiraishi T et al 2016 *Appl. Phys. Lett.* **108** 262904
- [32] Kracklauer M, Ambriz-Vargas F, Kolhatkar G, Huber B, Schindler C and Ruediger A 2019 *Adv. Mater. Lett.* **10** 405–9
- [33] Dong Z, Cao X, Wu T and Guo J 2018 *J. Appl. Phys.* **123** 094501